Supplementary Information for:

The role of carbon precursor on carbon nanotube chirality in floating catalytic chemical vapour deposition

J. S. Barnard, C. Paukner and K.K. Koziol.

Contents

Raman spectra of toluene, ethanol and methane grown CNTs

Raman spectroscopy was performed on Bruker Senterra Raman microscope using a HeNe laser (wavelength = 633 nm) with 2 mW of power. We used a 50× objective lens and acquired Raman spectra with 100 sec exposure. All CNT fibres were stretched and taped to glass slides for the analysis.

Table S1 summarizes the results of Gaussian fitting the radial breathing modes (RBM) between 100 and 250 cm^{-1} Stokes shift. D:G and and 2D:G ratios were used as proxy measures of the cleanliness of the CNT yarn.

RBM position at wave number (ω) in cm^{-1} and with intensity ratio over G peak together with corresponding tube diameter via $d_t = 227/\omega$.

D/G and 2D/G are intensity ratios of the respective peaks.

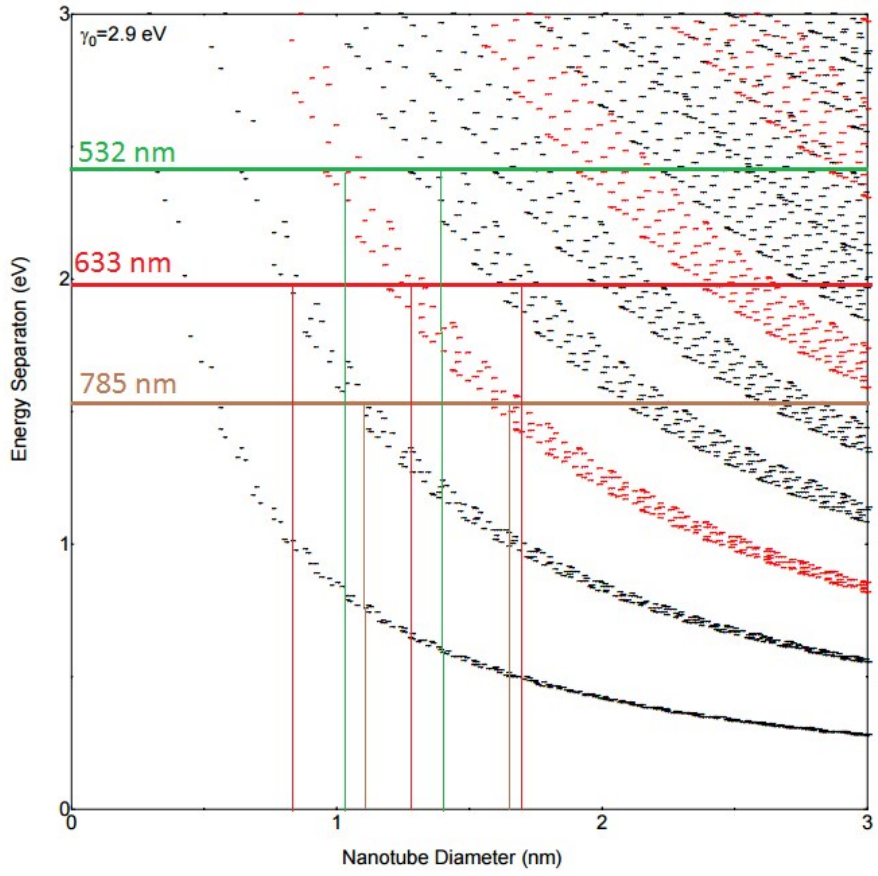

Figure S1.Kataura plot showing the laser energies and the tubes in near-resonant conditions for RBM exciation. Taken from:

http://www.photon.t.u-tokyo.ac.jp/~maruyama/kataura/kataura.html

Raman spectra of carbon nanotubes synthesized with ethanol

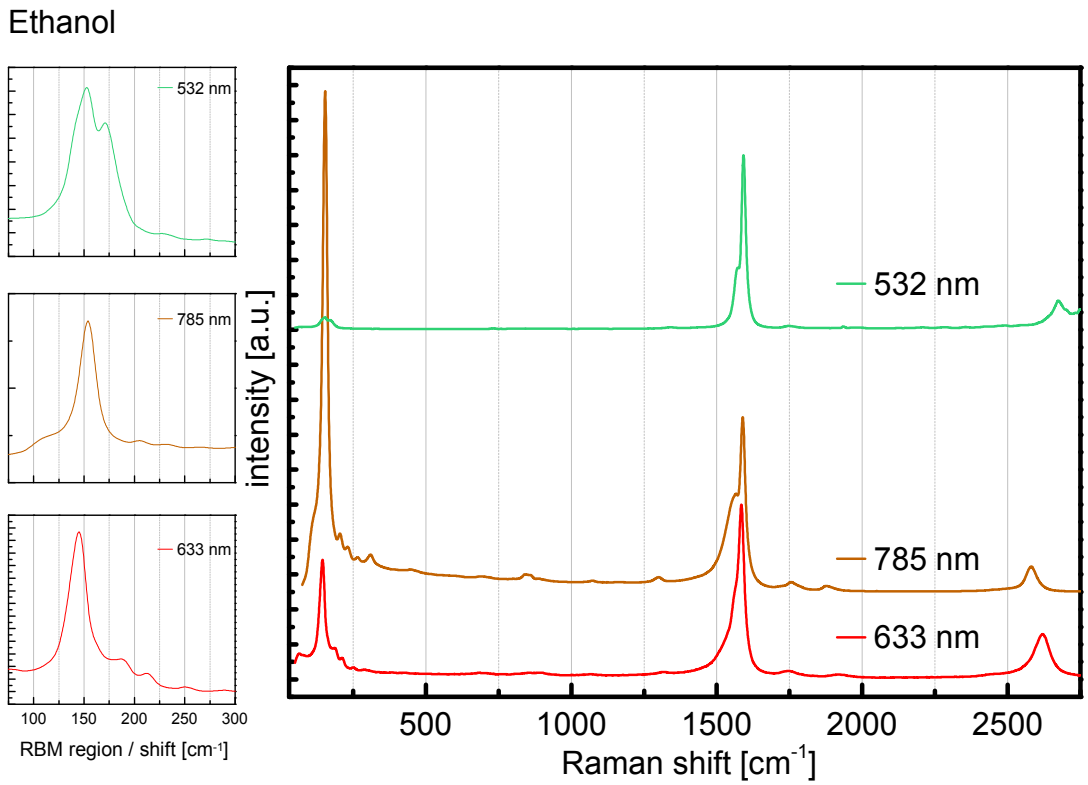

Figure S2. Raman spectra of the ethanol sourced CNTs from different laser lines, and scaled to give a normalised G peak (Intensity of line G is unity). The regions of the Raman spectra corresponding to the radial breathing modes are elaborated on the left hand side.

	RBM [cm^{-1}] (RBM:G)	d_T (nm)	D:G	2D:G
633 nm	145 (0.68)	1.6	0.04	0.26
	186.5 (0.18)	1.2	-	-
	212 (0.12)	1.1	-	-
	249.5 (0.07)	0.9	-	-
532 nm	153 (0.07)	1.5	-	0.17
	170.5 (0.06)	1.3	-	-
785 nm	154 (2.87)	1.5	-	0.15
	205 (0.33)	1.1	-	-
	231 (0.26)	1.0	-	-
	265 (0.20)	0.9	-	-

Table T1. Radial breathing mode frequencies and intensity ratios for ethanol with D-line, 2D-line to G-line ratios for ethanol.

Raman spectra of carbon nanotubes synthesized with methane

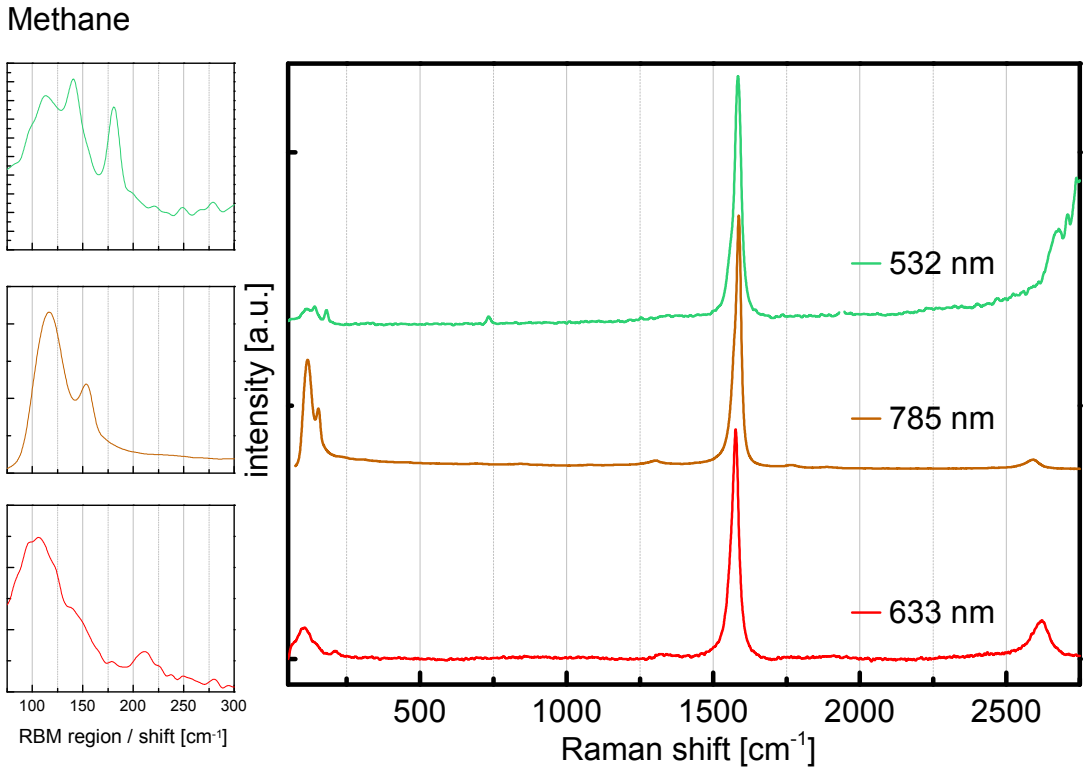

Figure S3 Raman spectra of the methane sourced CNTs from three different laser lines, and scaled to give a normalised G peak (Intensity of line G is unity). The regions of the Raman spectra corresponding to the radial breathing modes are elaborated on the left hand side.

	RBM [cm^{-1}] (RBM:G)	d_T (nm)	D:G	2D:G
633 nm	106 (0.19)	2.1	0.10	0.28
532 nm	113.5 (0.08)	2.0	-	0.45
	141 (0.09)	1.6	-	-
	180.5 (0.08)	1.3	-	-
785 nm	116.5 (0.43)	1.9	0.03	0.04
	153.5 (0.24)	1.5	-	-

Table T2. Radial breathing mode frequencies and intensity ratios for ethanol with D-line, 2D-line to G-line ratios for methane.

Raman spectra of carbon nanotubes synthesized with toluene

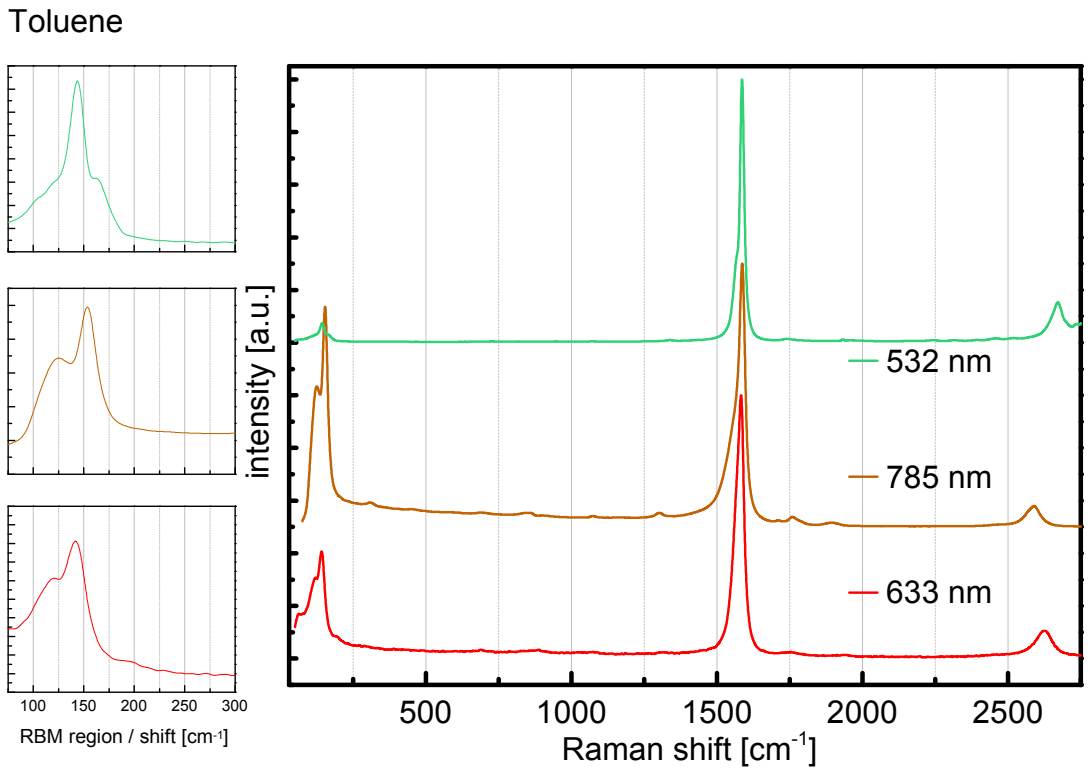

Figure S4. Raman spectra of the toluene sourced CNTs from different laser lines, and scaled to give a normalised G peak (Intensity of line G is unity). The regions of the Raman spectra corresponding to the radial breathing modes are elaborated on the left hand side.

	RBM [cm^{-1}] (RBM:G)	d_T (nm)	D:G	2D:G
633 nm	120.5 (0.31)	1.9	0.02	0.11
	141.5 (0.41)	1.6	-	-
532 nm	143.5 (0.07)	1.6	-	0.15
785 nm	125 (0.53)	1.8	0.05	0.08
	153.5 (0.84)	1.5	-	-

Table T3. Radial breathing mode frequencies and intensity ratios for ethanol with D-line, 2D-line to G-line ratios for toluene.

DWNT outer CNT chirality maps

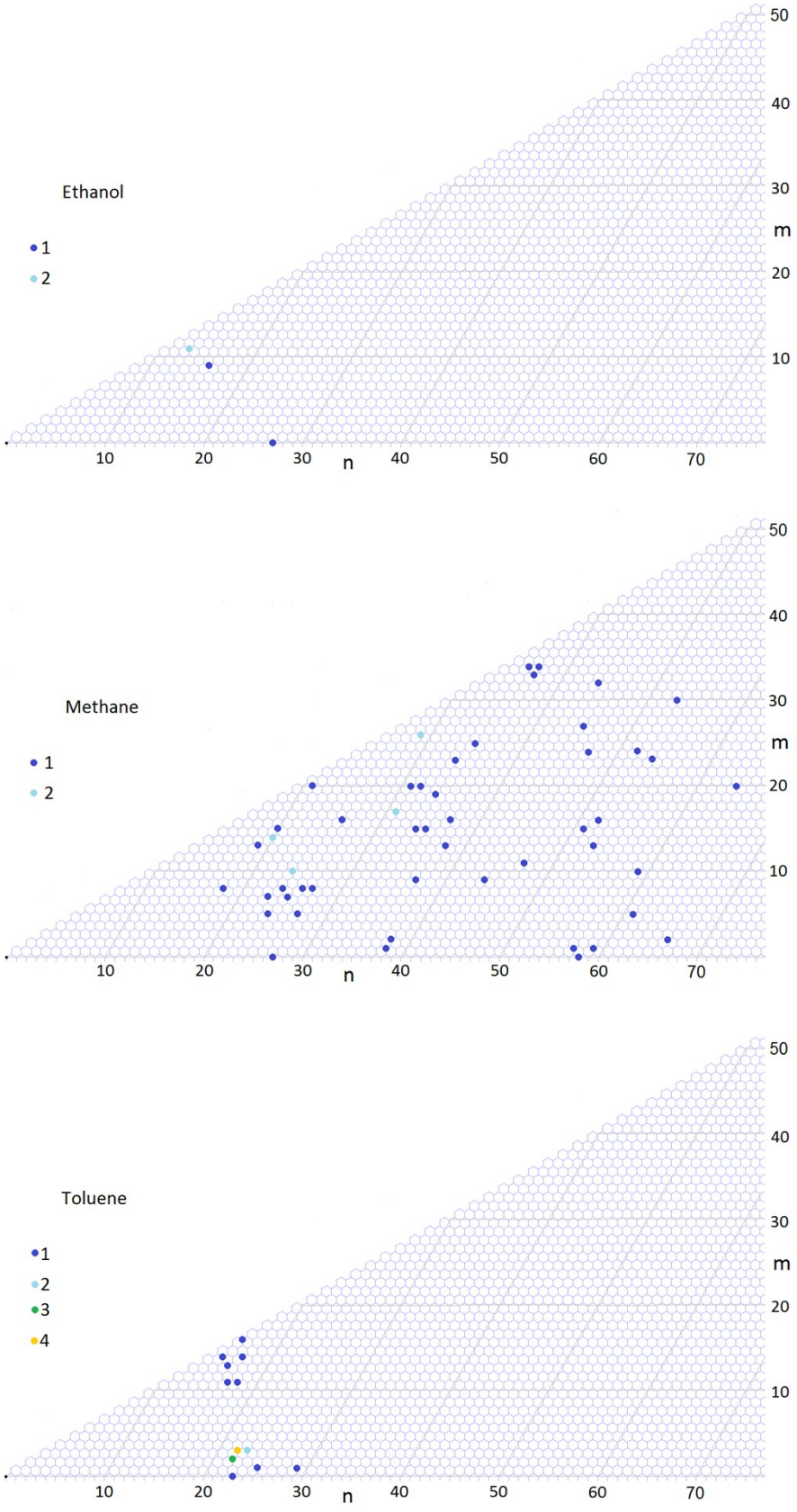

Figure S5. CNT chirality maps for the outer carbon nanotubes for DWNTs only.

SWNT and inner CNT diameter distributions

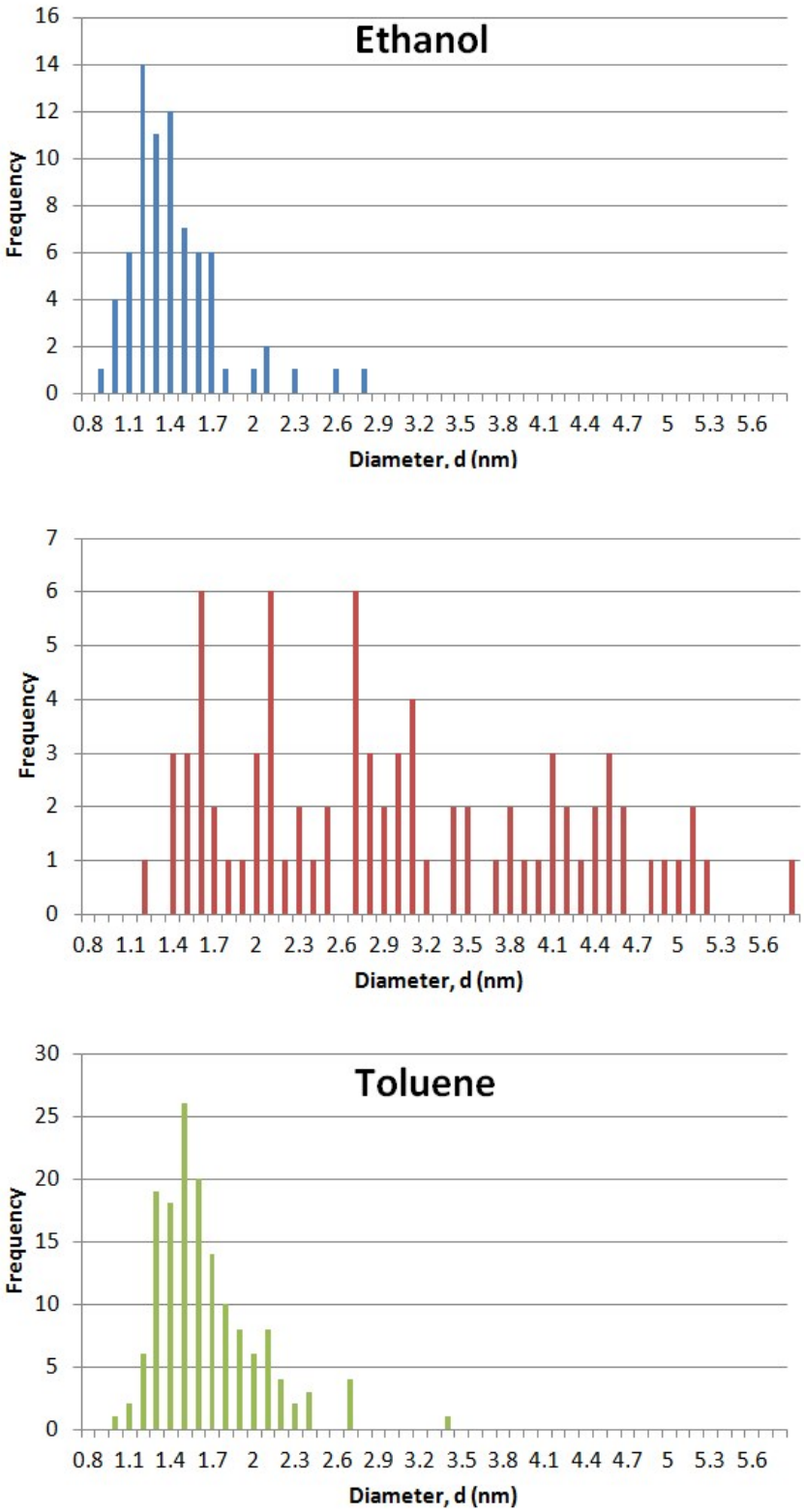

Figure S6. The frequency distribution of the diameters of CNTs seen for inner (for DWNT) and SWNT s only. All counts are in 0.1 nm bins.

Outer CNT diameter distributions

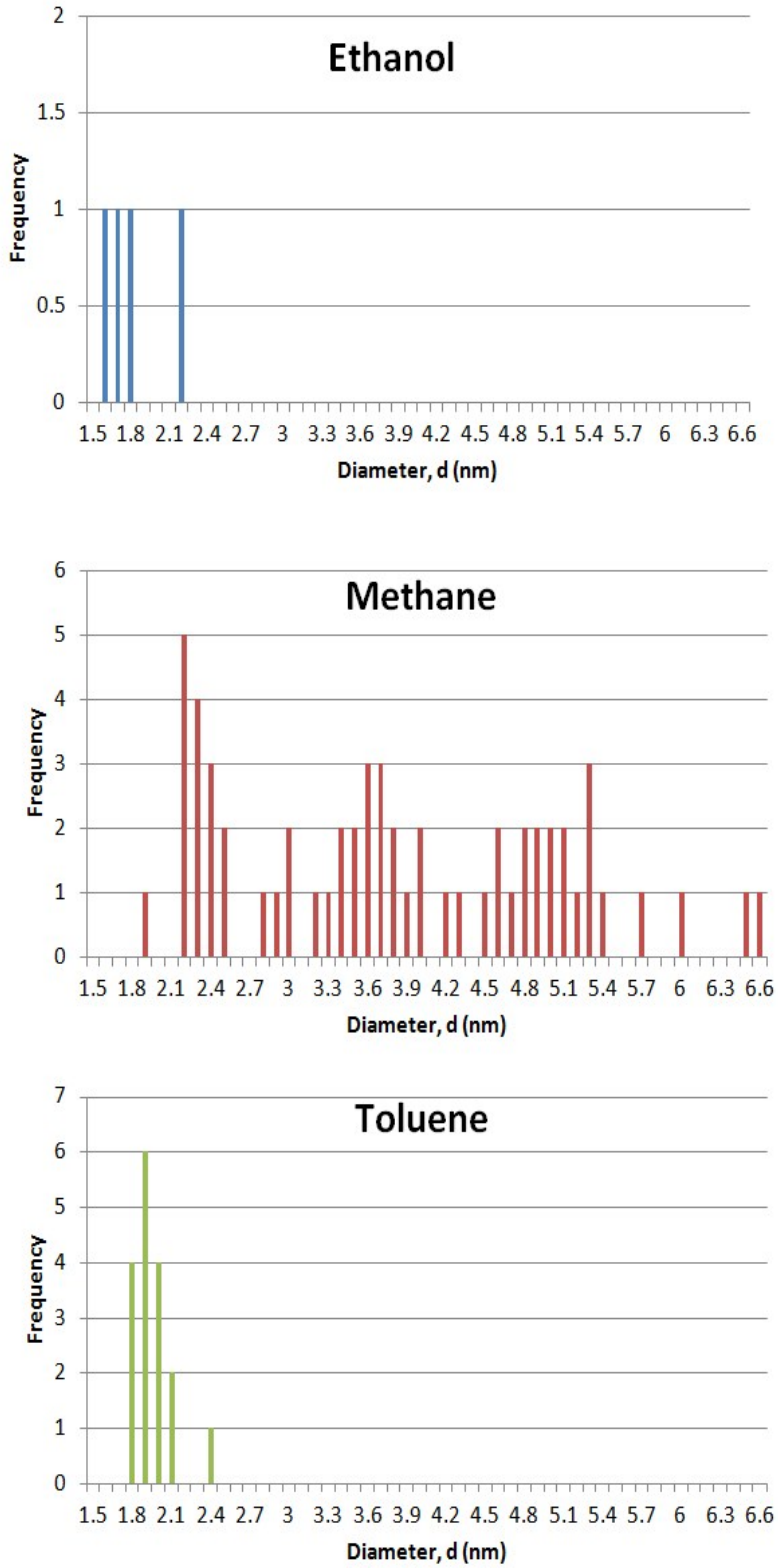

Figure S7. The frequency distribution of the diameters of CNTs seen for the outer tubes of DWNT s only. All counts are in 0.1 nm bins.

Metallic and semiconducting CNT statistics

	SWNT		DWNT				All tubes		S:M
	S	M	S@S	M@S	S@M	M@M	S	M	(error)
Ethanol	49	21	3	0	0	1	55	23	2.4(0.6)
Methane	11	7	21	13	11	12	77	55	1.4(0.2)
Toluene	87	50	7	6	3	1	110	61	1.8(0.3)

The error on the semiconducting-to-metal ratio, $\Delta_{S:M}$ is given by:

$$\Delta_{S:M} = \sqrt{\left(\left(\frac{\Delta_S}{N_M}\right)^2 + \left(\frac{\Delta_M N_S}{N_M^2}\right)^2\right)}$$

Where Δ_S and Δ_M, are the errors in the number of semiconducting and metallic CNTs, respectively. These may be taken to be Poisson distributed, i.e. $\Delta_S=\sqrt{N_S}$, etc.

Obtaining electron diffraction patterns from individual CNTs

Step 1. In bright-field TEM, identify a location on the CNT fibre material with a promising number of tubes. In this sample the fibre is mounted on a holey carbon film attached to a copper mesh grid.

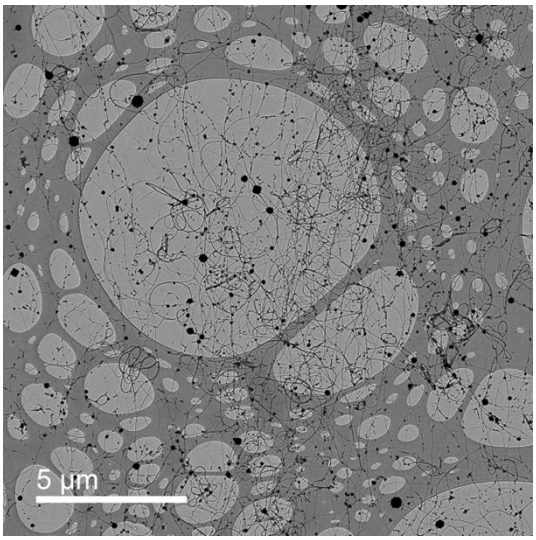

Step 2. Explore the fibre looking for candidate tubes. In this case two tubes are identified. The location is stored and the process repeated until a satisfactory number of tubes are located.

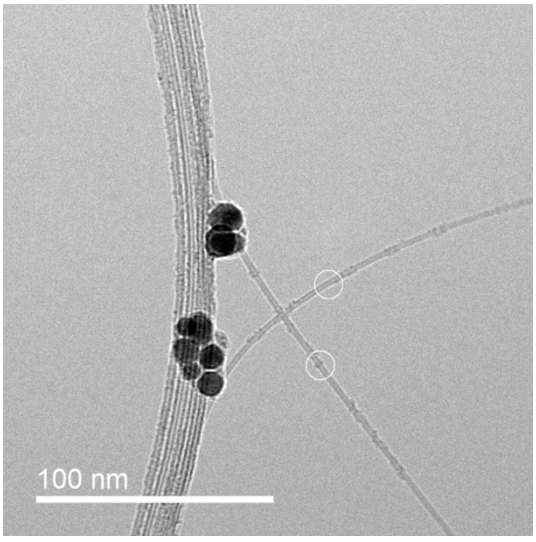

Two points are worth making:

1. Individual tubes should be close to, or emerge from bundles of tubes nearby.
2. Particles of iron residues should be used as tube location identifiers for the later STEM images.

Step 3. Switch the microscope to scanning TEM (STEM) with the same (finely collimated) electron probe used for diffraction. With a high-angle annular dark-field (HAADF) detector, find location of the individual CNTs, using the strong intensity of the iron particles to guide the process. Note: the blurriness of the image is due to the diffraction-limited nature of the probe and the low intensity is because of the low atomic number of the CNT.

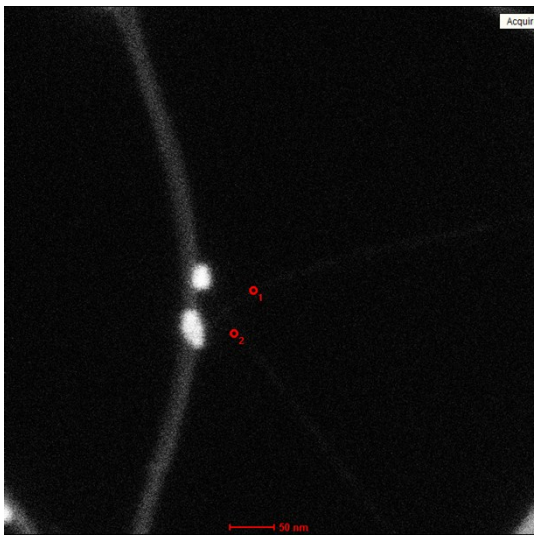

Step 4. Stop the electron probe scanning and manually direct the probe to sit, in turn, on each CNT. Acquire a diffraction pattern for each point. Note the near 90 degree rotation between equatorial lines, indicating that the CNTs from each pattern lie nearly perpendicular to each other.

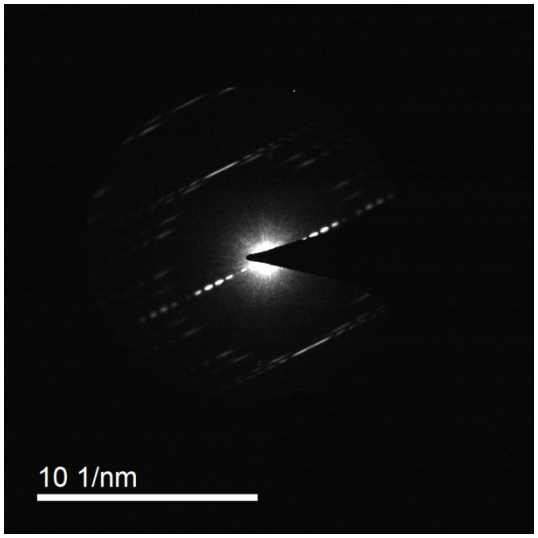

Diffraction point 1.

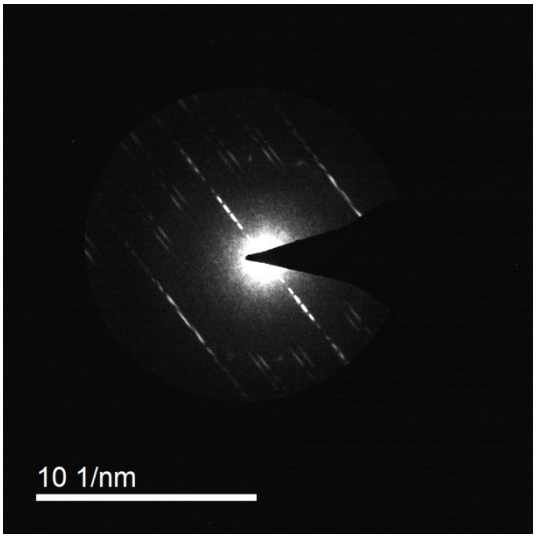

Diffraction point 2.

Step 5. Remove to the next stored location and repeat.

This concludes the Supplementary Information